Supporting Information

Yaeno et al. 10.1073/pnas.1106002108

SI Materials and Methods

Sample Preparation for NMR Spectroscopy. The ^{13}C,^{15}N-labeled protein was synthesized by the cell-free protein expression system (1). The expressed protein was purified by batch purification, using Ni Sepharose High Performance resin (GE Healthcare). The eluted protein was cleaved with tobacco etch virus protease to remove the His-tag and subsequently was exchanged into 20 mM Tris·HCl buffer (pH 7.0), containing 300 mM NaCl, 5 mM imidazole, and 1 mM tris(2-carboxyethyl)phosphine (TCEP), using a HiPrep 26/10 desalting column (GE Healthcare). The protein-containing fraction was applied to a HisTrap column, and its flow-through fraction was pooled. This fraction was exchanged into 20 mM Tris·HCl buffer (pH 7.0) containing 50 mM NaCl and 1 mM TCEP with a HiPrep 26/10 desalting column and was fractionated using a HiTrapSP cation exchange column (GE Healthcare) with a linear gradient of 0.05–1 M NaCl in 20 mM Tris·HCl buffer (pH 7.0) containing 1 mM TCEP. The purified protein was exchanged into the buffer (20 mM D-Tris·HCl (pH7.0) containing 100 mM NaCl, 1 mM D-DTT, 0.02% NaN_3, and 10% D_2O) with a VIVASPIN ultrafiltration device (Sartorius). The AVR3a4 domain sample consists of 108 amino acid residues. The first seven amino acid residues at the N terminus (GSSGSSG) are derived from the linker sequence used in the expression and purification system (2).

NMR Spectroscopy, Structure Determination, and Structural Analysis. The NMR spectra were recorded at 298 K on a Bruker AVANCE 700 MHz spectrometer equipped with a triple-resonance cryoprobe. The NMR sample contained 1.11 mM of uniformly ^{13}C,^{15}N-labeled *Phytophthora capsici* AVR3a4 in 20 mM D-Tris (pH 7.0), 300 mM NaCl, 1 mM D-DTT, 0.02% NaN_3, and 10% ^2H_2O/90% ^1H_2O. Resonance assignments were made using the standard NMR techniques (3, 4). The NMR spectra acquired for the resonance assignments were 2D ^1H-^{15}N heteronuclear single quantum coherence (HSQC) and ^1H-^{13}C HSQC and 3D HNCA, HN(CO)CA, HNCO, HN(CA)CO, HNCACB, CBCA(CO)NH, HBHA(CO)NH, C(CCO)NH, HC(C)H-TOCSY, (H)CCH-TOCSY, and HC(C)H-COSY. All spectra were processed using the NMRPipe software package (5). The programs KUJIRA (6) and NMRView (7, 8) were used for visualization of the NMR spectra and chemical shift assignments.

For the structure calculation, ^{15}N-edited NOESY and ^{13}C-edited NOESY with 80-ms mixing times were used to determine the distance restraints. Dihedral angle restraints were derived using the program TALOS (9). Automated NOE cross-peak assignments and structure calculations with torsion angle dynamics were performed using the program CYANA (10–13). One hundred structures were calculated, and the 20 structures with the lowest target function values in the final calculation cycle were selected. The stereochemical quality of the structures was assessed using the program PROCHECK-NMR (14). The statistics of the structures and the distance and torsion angle constraints used for the structure calculation are summarized in Table S1. The coordinates of AVR3a4 have been deposited in the Protein Data Bank (PDB ID: 2LC2), and the NMR chemical shifts have been deposited in the Biological Magnetic Resonance Bank (accession no. 17588).

Molecular Homology Modeling. The 3D structure of the AVR3a was built by comparative protein structure modeling with the program MODELLER-9v5 (15–17). The input consisted of the template structure (i.e., the solution structure of AVR3a4 determined by NMR) and the sequence alignment (shown in Fig. 1*A*) of each AVR3a4 homolog target with the template AVR3a4. Applying the default model-building routine model, 10 comparative models of the target sequence were built by MODELER; the model with the lowest value of the Modeler objective function was selected as the best model. The stereochemical qualities of the model were checked by PROCHECK (18).

Plasmid Construction. The construct to express the mature AVR3a protein for NMR analysis was generated using two-step PCR (19). For the lipid-binding assay or *in planta* expression, the 5′ primer 5′-CAC CAT GGA CCA GAC CAA AGT ACT GGT ATA-3′ was used in combination with the 3′ primer 5′-GAG CTC ATA CCC GGT TAA CCC CAG ATG C-3′ or with the 3′ primer 5′-TCA ATA CCC GGT TAA CCC CAG ATG C-3′ to amplify the *Avr3a* fragments. The resulting fragments were cloned into pENTR/SD-TOPO or pENTR/D-TOPO vectors (Invitrogen). pENTR constructs with amino acid substitutions in the positively charged area were generated using the GeneTailor Site-Directed Mutagenesis System (Invitrogen). The fragments were cloned into pDEST17, pDEST24 (Invitrogen), or pGWB12 vectors for the expression of the N-terminal His-tagged proteins, C-terminal GST fusion proteins, or N-terminal FLAG-tagged AVR3a *in planta*, respectively. The *Arabidopsis PIP5K1* gene was cloned into pEAQ-HT vector (20) with the In-Fusion system (Clontech) using the 5′ primer 5′-CAT CAC CAT CAT CCC GAA CAC CTG TAT TTT CAG GGA ATG AGT GAT TCA G-3′ and the 3′ primer 5′-ACC AGA GTT AAA GGC CTC GAG TTA GCC CTC TTC AAT GAA G-3′. For the construction of AVR3a4 variants, the 5′ primer 5′-CAC CAT GAA TGT GGA CTC GAA CCA AAA CAA-3′ and the 3′ primer 5′-GAG CTC ATA ATC CAG GTG GAT CAC AT-3′ were used to amplify the *AVR3a4* fragments. The 3′ primer 5′-GCC AAG TTG AAG TTG GGA GCT CGT TCC TCC GTG TCG GAC T-3′ and the 5′ primer 5′-AAG AGA CCA GCG AGG AGC GTG GCT TCT TAG AGA AGG CGG C-3′ or the 3′ primer 5′-GTC CGC CAG TTT ATC GTT ACC CAT AAT TGC CTT GGC CAT TTT C-3′ and the 5′ primer 5′-GAA AAT GGC CAA GGC AAT TAT GGG TAA CGA TAA ACT GGC GGA C-3′ were used to make chimera constructs for AVR3a4 (N22-R58)–AVR3a (A60-Y147) and AVR3a4 (N22-M74)–AVR3a (G93-Y147), respectively. The resulting fragment was cloned into pENTR/SD-TOPO vector (Invitrogen). The fragments were cloned into pDEST24 vector (Invitrogen) for the expression of C-terminal GST fusion proteins.

Protein Expression and Purification. *Escherichia coli* strain BL21-AI (Invitrogen) was transformed with the pDEST17 or the pDEST24 vector encoding *Avr3a* and its variants. Cultures were grown to OD_{600} of 0.5 before protein expression was induced by adding 0.2% arabinose and incubation at 28 °C for 3 h. Cells were pelleted and lysed by sonication in the ice-cold lysis buffer (20 mM Tris·HCl, 500 mM NaCl, 20 mM imidazole, pH 8.0, for His-tagged protein or 10 mM Na_2HPO_4, 1.8 mM KH_2PO_4, 140 mM NaCl, 2.7 mM KCl, pH 7.3, for GST fusion protein). The supernatants of the cell lysates were added to a HisTrap HP column or GSTrap HP column on an ÄKTA Explorer 10S System (GE Healthcare). His-tagged proteins were separated by linear gradient elution with 20 mM Tris·HCl, 500 mM NaCl, 500 mM imidazole, pH 8.0. GST fusion proteins were separated by stepwise elution with 50 mM Tris·HCl, 10 mM reduced glutathione, pH8.0. All purification steps were carried out at 4 °C.

Lipid-Binding Assay. Nitrocellulose membranes spotted with 100 pmol of phospholipids (PIP Strips; Echelon Biosciences) were blocked in 1% nonfat milk in PBS for 1 h and then incubated with 1 μg/mL GST-fusion proteins overnight at 4 °C. The membranes were washed with PBS containing 0.1% Tween 20 (PBS-T) and incubated for 1 h with anti–GST-HRP antibody (GE Healthcare) diluted to 1:2,000. Finally, the membranes were washed with PBS-T, and GST-fusion proteins bound to phosphatidylinositol monophosphates (PIPs) were detected by ECL Plus Immuno Blotting Detection Reagents (GE Healthcare). In addition to using PIP Strips from Echelon Biosciences, serial dilutions of PIPs were spotted on to nitrocellulose membranes, and lipid-binding assays were performed as described above. The membranes incubated with different proteins were washed for the same length of time and detected with the same exposure time in each experiment.

Agroinfiltration Assay. *Agrobacterium tumefaciens* GV3101 strains were grown in LB medium supplemented with kanamycin at 50 μg/mL Agroinfiltration experiments were performed on 3- to 5-wk-old *Nicotiana benthamiana* plants. Plants were grown and maintained throughout the experiments in a growth room at 20–25 °C under continuous fluorescent light. Coexpression of *R3a* and *Avr3a* by agroinfiltration was performed as follows. Strains carrying the pBINplus-R3a (21) and pGWB12-AVR3a constructs were mixed in a 2:1 ratio in induction buffer (10 mM MES, 10 mM $MgCl_2$, 200 μM acetosyringone, pH 5.6) to a final OD_{600} of 0.3. For the INF1-induced cell-death–suppression assays, sites infiltrated with strains carrying pGWB12-AVR3a constructs were challenged with the strain carrying p35S-INF1 at a final OD_{600} of 0.3 in induction buffer. For immunoblot analyses, leaves of *N. benthamiana* were coinfiltrated with *A. tumefaciens* carrying pGWB12-AVR3a constructs with or without the pGWB18-CMPG1 construct, which contains *CMPG1* (*Solanum tuberosum StCMPG1b*) (22), in combination with pJL3-p19 for expression of the suppressor of posttranscriptional gene silencing p19 of the tomato bushy stunt virus (23). In a similar way, strains carrying the pEAQ-HT-PIP5K1 constructs or pEAQ-HT empty vector were infiltrated into 3-wk-old *N. benthamiana* leaves 2 d before infiltration of the strain carrying pGWB12-AVR3a. Four days later, the infiltrated sites were harvested for immunoblot analyses or were challenged further with the strain carrying p35S-INF1 for the INF1-induced cell-death–suppression assays.

Immunoblot Analyses. Leaf tissues were harvested 5 d post-infiltration and were ground in liquid nitrogen followed by boiling for 5 min in SDS-loading buffer supplemented with 50 μM DTT. The extracted proteins were separated by SDS/PAGE followed by transfer to nitrocellulose membranes and immunodetection using anti–myc-HRP antibodies (Santa Cruz) diluted 1:4,000 for CMPG1; anti-FLAG M2-HRP antibodies (Sigma-Aldrich) diluted 1:8,000 for AVR3a; anti-H^+-ATPase antibodies (Agrisera) diluted 1:2,000 as a plasma membrane marker; and anti-UDPase antibodies (Agrisera) diluted 1:2,000 as a cytoplasm marker. The detection was performed using SuperSignal West Femto Maximum Sensitivity Substrate (Thermo Scientific) for CMPG1, ECL immunoblotting detection reagents (GE Healthcare) for AVR3a, and ECL Plus immunoblotting detection reagents (GE Healthcare) for H^+-ATPase and UDPase.

Circular Dichroism. The circular dichroism spectra of AVR3a and $AVR3a^{K85E}$ were recorded at 4 °C on a J-820 Spectropolarimeter (Jasco). Data were collected in 1-nm increments (20 nm/min) by using cuvettetes with a 0.2-cm path length, a 4-s averaging time, and 1-nm bandwidth. Proteins were dissolved in 20 mM Tris·HCl (pH 7.0) and 100 mM NaCl, and their solutions were adjusted to an A280 of 0.3. Protein concentration was determined from A280 values, and molar absorption coefficients were calculated from the amino acid sequences.

Yeast Two-Hybrid Assay. The fragments of *Avr3a* and *ΔN-StCMPG1b* were cloned into the EcoRI-PstI cloning site of pBTM116 and pVP16, respectively, and the yeast two-hybrid assay was performed as described by Bos et al. (22) and Ulm et al. (24).

1. Matsuda T, et al. (2007) Improving cell-free protein synthesis for stable-isotope labeling. *J Biomol NMR* 37:225–229.
2. Yabuki T, et al. (2007) A robust two-step PCR method of template DNA production for high-throughput cell-free protein synthesis. *J Struct Funct Genomics* 8:173–191.
3. Wüthrich K (1986) *NMR of Proteins and Nucleic Acids* (John Wiley & Sons, New York).
4. Cavanagh J, Fairbrother W, Palmer A, Skelton N (1996) *Protein NMR Spectroscopy. Principles and Practice* (Academic, New York).
5. Delaglio F, et al. (1995) NMRPipe: A multidimensional spectral processing system based on UNIX pipes. *J Biomol NMR* 6:277–293.
6. Kobayashi N, et al. (2007) KUJIRA, a package of integrated modules for systematic and interactive analysis of NMR data directed to high-throughput NMR structure studies. *J Biomol NMR* 39:31–52.
7. Johnson BA (2004) Using NMRView to visualize and analyze the NMR spectra of macromolecules. *Methods Mol Biol* 278:313–352.
8. Johnson B, Blevins R (1994) NMR View: A computer program for the visualization and analysis of NMR data. *J Biomol NMR* 4:603–614.
9. Cornilescu G, Delaglio F, Bax A (1999) Protein backbone angle restraints from searching a database for chemical shift and sequence homology. *J Biomol NMR* 13: 289–302.
10. Güntert P, Mumenthaler C, Wüthrich K (1997) Torsion angle dynamics for NMR structure calculation with the new program DYANA. *J Mol Biol* 273:283–298.
11. Herrmann T, Güntert P, Wüthrich K (2002) Protein NMR structure determination with automated NOE assignment using the new software CANDID and the torsion angle dynamics algorithm DYANA. *J Mol Biol* 319:209–227.
12. Jee J, Güntert P (2003) Influence of the completeness of chemical shift assignments on NMR structures obtained with automated NOE assignment. *J Struct Funct Genomics* 4:179–189.
13. Güntert P (2004) Automated NMR structure calculation with CYANA. *Methods Mol Biol* 278:353–378.
14. Laskowski RA, Rullmannn JA, MacArthur MW, Kaptein R, Thornton JM (1996) AQUA and PROCHECK-NMR: Programs for checking the quality of protein structures solved by NMR. *J Biomol NMR* 8:477–486.
15. Sali A, Blundell TL (1993) Comparative protein modelling by satisfaction of spatial restraints. *J Mol Biol* 234:779–815.
16. Martí-Renom MA, et al. (2000) Comparative protein structure modeling of genes and genomes. *Annu Rev Biophys Biomol Struct* 29:291–325.
17. Fiser A, Sali A (2003) Modeller: Generation and refinement of homology-based protein structure models. *Methods Enzymol* 374:461–491.
18. Laskowski R, MacArthur M, Moss D, Thornton J (1993) PROCHECK: A program to check the stereochemical quality of protein structures. *J Appl Cryst* 26:283–291.
19. Yabuki T, et al. (2007) A robust two-step PCR method of template DNA production for high-throughput cell-free protein synthesis. *J Struct Funct Genomics* 8:173–191.
20. Sainsbury F, Thuenemann EC, Lomonossoff GP (2009) pEAQ: Versatile expression vectors for easy and quick transient expression of heterologous proteins in plants. *Plant Biotechnol J* 7:682–693.
21. Huang S, et al. (2005) Comparative genomics enabled the isolation of the R3a late blight resistance gene in potato. *Plant J* 42:251–261.
22. Bos JIB, et al. (2010) *Phytophthora infestans* effector AVR3a is essential for virulence and manipulates plant immunity by stabilizing host E3 ligase CMPG1. *Proc Natl Acad Sci USA* 107:9909–9914.
23. Voinnet O, Rivas S, Mestre P, Baulcombe D (2003) An enhanced transient expression system in plants based on suppression of gene silencing by the p19 protein of tomato bushy stunt virus. *Plant J* 33:949–956.
24. Ulm R, et al. (2002) Distinct regulation of salinity and genotoxic stress responses by Arabidopsis MAP kinase phosphatase 1. *EMBO J* 21:6483–6493.

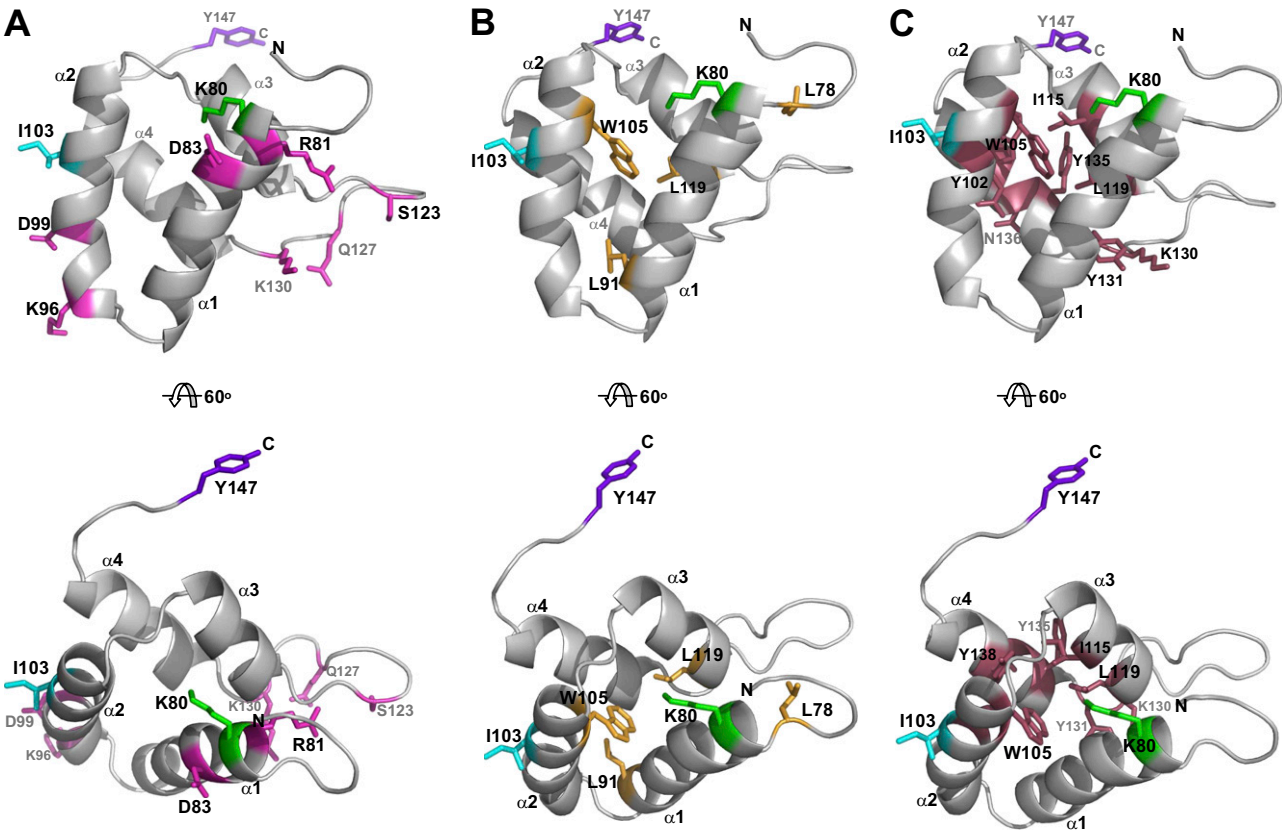

Fig. S1. Positions of potent amino acid residues of AVR3a. (*A*) Amino acids whose substitution can confer gain-of-function mutations (magenta) are mapped on the ribbon diagram of AVR3a. (*B*) Amino acids whose substitution can cause loss-of-function mutations (orange) are mapped on the ribbon diagram of AVR3a. (*C*) Amino acids comprising the W and Y motifs which have been postulated by Dou et al. (1) (dark red and purple) are mapped on the ribbon diagram of AVR3a (K80, green; I103, cyan; Y147, purple).

1. Dou D, et al. (2008) RXLR-mediated entry of *Phytophthora sojae* effector Avr1b into soybean cells does not require pathogen-encoded machinery. *Plant Cell* 20:1930–1947.

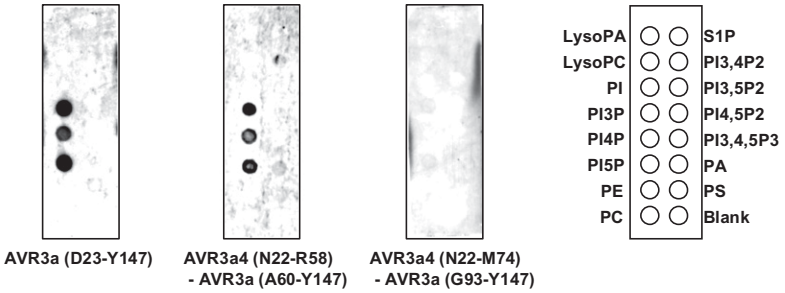

Fig. S2. Protein lipid overlay assay of chimera proteins of AVR3a and AVR3a4. The RXLR domain of AVR3a4 (Asn22–Arg58) was fused with the effector domain of AVR3a (Ala60–Y147) or the RXLR domain, and the α1 helix of AVR3a4 (Asn22–Met74) was fused with the α2–α4 helices of AVR3a (Gly93–Tyr147). The lipid overlay assay was performed as in Fig. 2*A*. PA, phosphatidic acid; PC, phosphatidylcholine; PE, phosphatidylethanolamine; PI, phosphatidylinositol; PI3P, PI-3-phosphate; PI4P, PI-4-phosphate; PI5P, PI-5-phosphate; PI3,4P2, PI-3,4-biphosphate; PI3,5P2, PI-3,5-biphosphate; PI4,5P3, PI-4,5-biphosphate; PI3,4,5P3, PI-3,4,5-triphosphate; PS, phosphatidylserine; S1P, sphingosine-1-phosphate.

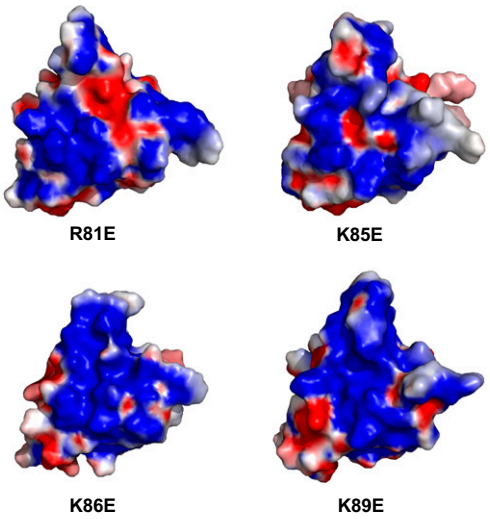

Fig. S3. Surface charge distribution of AVR3a^{R81E}, AVR3a^{K85E}, AVR3a^{K86E}, and AVR3a^{K89E}. The surface charge distribution of each mutant was calculated with PyMol (DeLano Scientific). Positively and negatively charged surfaces are shown in blue and red, respectively.

Table S1. Summary of the conformational restraints and statistics of the final 20 best structures

NOE upper distance limits	
Total	1528
Intra residue ($\|i - j\| = 0$)	491
Sequential ($\|i - j\| = 1$)	335
Medium range ($1 < \|i - j\| < 5$)	356
Long range ($\|i - j\| \geq 5$)	346
Torsion angle restraints	90
CYANA target function value	0.0208
Distance restraint violations	
Number > 0.1 Å	0
Maximum (Å)	—
Torsion angle restraint violations	
Number > 5°	0
Maximum (°)	—
PROCHECK*	
Residues in favored regions	87.4%
Residues in additionally allowed regions	12.2%
Residues in generously allowed regions	0.4%
Residues in disallowed regions	0.0%
RMS deviation to the averaged coordinates	
All regions†	
Backbone atoms (Å)	0.54
Heavy atoms (Å)	0.94
Ordered regions‡	
Backbone atoms (Å)	0.36
Heavy atoms (Å)	0.83

*The region for the PROCHECK calculation includes F60–Y122.
† "All regions" include F60–Y122.
‡"Ordered regions" include F60–A75, K79–K90, L94–F100, and D110–D121.